Send Orders for Reprints to reprints@benthamscience.net

Current Computer-Aided Drug Design, XXXX, *XX,* 0-0

RESEARCH ARTICLE

In silico Study on Natural Chemical Compounds from Citric Essential Oils as Potential Inhibitors of an Omicron (BA.1) SARS-CoV-2 Mutants' Spike Glycoprotein

Olha Ovchynnykova[1], Jordhan D. Booth[2], Trey M. Cocroft[2], Kostyantyn M. Sukhyy[1] and Karina Kapusta[2,*]

[1]*Ukrainian State University of Chemical Technology, Dnipro, 49005, Ukraine;* [2]*Department of Chemistry and Physics, Tougaloo College, Tougaloo, MS, 39174, USA*

ARTICLE HISTORY

Received: August 21, 2023
Revised: November 22, 2023
Accepted: November 27, 2023

DOI:
10.2174/0115734099275132231213055138

Abstract: ***Background*:** SARS-CoV-2's remarkable capacity for genetic mutation enables it to swiftly adapt to environmental changes, influencing critical attributes, such as antigenicity and transmissibility. Thus, multi-target inhibitors capable of effectively combating various viral mutants concurrently are of great interest.

***Objectives*:** This study aimed to investigate natural compounds that could unitedly inhibit spike glycoproteins of various Omicron mutants. Implementation of various *in silico* approaches allows us to scan a library of compounds against a variety of mutants in order to find the ones that would inhibit the viral entry disregard of occurred mutations.

***Methods*:** An extensive analysis of relevant literature was conducted to compile a library of chemical compounds sourced from citrus essential oils. Ten homology models representing mutants of the Omicron variant were generated, including the latest 23F clade (EG.5.1), and the compound library was screened against them. Subsequently, employing comprehensive molecular docking and molecular dynamics simulations, we successfully identified promising compounds that exhibited sufficient binding efficacy towards the receptor binding domains (RBDs) of the mutant viral strains. The scoring of ligands was based on their average potency against all models generated herein, in addition to a reference Omicron RBD structure. Furthermore, the toxicity profile of the highest-scoring compounds was predicted.

***Results*:** Out of ten built homology models, seven were successfully validated and showed to be reliable for *in silico* studies. Three models of clades 22C, 22D, and 22E had major deviations in their secondary structure and needed further refinement. Notably, through a 100 nanosecond molecular dynamics simulation, terpinen-4-ol emerged as a potent inhibitor of the Omicron SARS-CoV-2 RBD from the 21K clade (BA.1); however, it did not show high stability in complexes with other mutants. This suggests the need for the utilization of a larger library of chemical compounds as potential inhibitors.

***Conclusion*:** The outcomes of this investigation hold significant potential for the utilization of a homology modeling approach for the prediction of RBD's secondary structure based on its sequence when the 3D structure of a mutated protein is not available. This opens the opportunities for further advancing the drug discovery process, offering novel avenues for the development of multifunctional, non-toxic natural medications.

Keywords: SARS-CoV-2, spike glycoprotein receptor binding domain, homology modeling, molecular dynamics, citrus essential oil, terpinen-4-ol.

*Address correspondence to this author at the Department of Chemistry and Physics, Tougaloo College, Tougaloo, MS, 39174, USA; Tel: +1601-977-7792; E-mail: kkapusta@tougaloo.edu

1573-4099/XX $65.00+.00

1. INTRODUCTION

Different variants of severe acute respiratory syndrome coronavirus 2 (SARS-CoV-2) spread quickly around the world, causing severe acute respiratory syndrome disease (COVID-19) with high rates of morbidity and mortality and provoking a global economic crisis [1]. In the last few years, researchers have been interested in developing vaccines and drugs to stop the spread of the virus [2, 3]. In clinical trials, vaccines with mRNA, such as Pfizer-BioNTech and Moderna [4, 5], and vaccines with viral vectors, such as Johnson & Johnson and AstraZeneca [6, 7], have proven to be effective. However, the level of protection these vaccines can provide against the newest strains of the virus is still poorly understood [8-10]. During the SARS-CoV pandemic in 2003, tests were performed on infected patients and showed that the antibody response persisted for more than two years after infection [11]. According to Edridge *et al.* [12], the immunity against human coronavirus strains does not remain permanent, and reinfection is possible within six months. New emerging spike mutants of SARS-CoV-2 may hinder recognition by neutralizing antibodies, which may lead to more reinfections and reduced vaccine efficacy [13, 14].

On 26 November 2021, the World Health Organization (WHO) declared Omicron a global variant of concern (VOC) [15]. The existence of a huge number of mutations in its genomic sequence, specifically in the spike glycoprotein, raises the suspicion that Omicron could pose an epidemiological threat and cause another wave of COVID-19 on a global scale [16-18]. The Omicron strain appeared to be more contagious, but its clinical effects were less dangerous than those of Delta [19, 20]. As documented by the scientific literature [21, 22], Omicron is characterized by a less severe onset, lower rates, and shorter duration of hospitalization, as well as declining case fatality rates. Nonetheless, some experimental studies have shown that the Omicron variant is characterized by high immune escape, which provokes a decrease in the efficiency of vaccines [13, 23, 24]. These data are consistent with the rapid spread of the Omicron strain and increased incidence in countries and regions with high percentages of vaccinated populations [25]. At first, the vast majority of the virus genetic sequences detected in patients belonged to subspecies BA.1, which has shown substantial escape from neutralizing antibodies induced by vaccination [26]. One of the further Omicron mutants was characterized by low detection by test systems and has been called "stealth". This BA.2 sub-lineage has increased mutations and a defect in the spike gene deletion in the 69-70 sequence region, which indicates that it will not be identified by the S Gene Target Failure (SGTF) assay [27]. The number of BA.2 mutants has been increasing since the second half of January 2022, and now it has branched into new sublineages, such as BA.5, BQ.1, BA.2.75, XBB, XBB.1.5, XBB.1.16, *etc*. [28]. Mutations occurring in the receptor binding domain (RBD) of novel variants have different effects on its binding to human receptors, including ACE2 and human neutralizing antibodies, and its inhibition by drugs. For all that, not only the current vaccines should be consistently improved, but also new antiviral drugs must be rapidly developed. Thus, it is of great importance to consider mutations of a virus in the drug discovery process.

A series of studies used a computational approach to investigate the binding strength of Omicron RBD to the ACE2 receptor [29-32], therapeutic antibodies [24, 33, 34], and various drug candidates [32, 35-37]. In [32], it was computationally evaluated that the inhibitors of Omicron RBD should be acidic compounds, such as m-carboxyl-L-tyrosine, citric acid, citric acid glycosides, ferulic acid, gallic acid, glycyrrhizic acid, ibuprofen, lactic acid, malic acid, mefenamic acid, nalidixic acid, and naproxen, which would repulse from ACE-2 in a contact site. High-molecular-weight compounds, such as heparin oligosaccharides and desulphated heparins, also showed a potency for preventing viral entry of some Omicron clades (BA.2.12.1, BA.4, and BA.5) as it was shown by a combined experimental and computational study in [37]. The use of peptide inhibitors was evaluated computationally [38] for BA.1, BA.2, and BA.3 subvariant and, as a result, five antiviral peptides (AVP1056, AVP1059, AVP1225, AVP1801, and HIP755) were proposed to potentially hinder omicron-host interactions. It must be noted that the vast majority of studies involve only several variants as targets, which does not provide a full picture of how mutations may influence the success of the drug-design process. In [39], a large number of mutants, including Alpha, Beta, Delta, and Omicron (BA.1, BA.2, BA.2.75. BA.2.75.2, BA.5, BQ.1.1, XBB, XBB.1.5) variants, was used as targets for the development of SARS-CoV-2-neutralizing antibodies against Omicron subvariants.

To perform an accurate computational elucidation of a such type, the 3D structure availability is crucial. This puts forward another computational approach, namely homology modeling, as a useful tool [40]. In our previous work [41], the methodology for the efficient discovery of potent inhibitors targeting mutant RBDs of SARS-CoV-2 was proposed and tested. This work featured a combination of homology modeling, molecular docking, molecular mechanics, and molecular dynamics simulations to scan a library of active ingredients from Traditional Chinese Medicines. We identified three lead compounds present in citrus essential oils (hesperidin, narirutin, and neohesperidin) suitable for multitarget SARS-CoV-2 inhibition; however, none of these compounds showed efficacy in targeting an Omicron variant. Due to their antiviral and immune-strengthening properties, natural compounds can serve as promising candidates for preventing COVID-19 infection. The purpose of this study is to investigate the potential of natural compounds from citrus essential oils against the Omicron lineage of SARS-CoV-2. Of particular interest is the ability of natural compounds to inhibit the RBD of a spike glycoprotein, which might prevent the virus from binding to its entry point ACE-2 receptors. To test the effectiveness of the proposed ligands, we built homology models of multiple clades of the Omicron variant. Molecular docking and molecular dynamics were used to test natural compounds and identify those that have the greatest potential of inhibiting various mutants simultaneously.

2. MATERIALS AND METHODS

2.1. Protein Preparation and Homology Modelling

The spike glycoprotein receptor binding domains of the Wild Type SARS-CoV-2 and its Omicron variants were cho-

sen for this work as reference. The 3D structures with PDB IDs: 6M0J (Wild-Type), 7T9L (21K or BA.1), 7XAZ (21K R346K mutant or BA.1.1), 7XB0 (21L), 7XWA (22B), 7XNS (22C), and 8IF2 (22E) were retrieved from the Protein Databank (https://www.rcsb.org/). The Schrodinger software package was used for all calculations [42]. We used Protein Preparation Wizard [43] to prepare the RBD structures for further simulations. All crystallographic water molecules were removed. Hydrogen atoms were added after the removal of the original Hydrogen atoms. Protonation states at target physiological pH = 7.4 ± 0.0 were generated using the Epik program [44]. To ensure a consistent and robust protein structure, we minimized the hydrogen bond network and optimized the structures using the OPLS3e force field [45]. Further, chain A containing RBD was extracted from the structure of Omicron RBD and ACE2 complex (PDB ID: 7T9L) and was used as a template for homology modeling of mutants represented as clades 21K, 21L, 22A, 22B, 22C, 22D, 22E, 22F, 23C, and 23F. Mutations for each clade were collected from the GISAID database [28] (https://nextstrain.org/ncov/gisaid/global/6m) and are illustrated in Table **1**. Schrodinger Software Package was used to build Homology Models with the ClustalW alignment method [46] and Loop Refinement using Prime Module. All models were built using an energy-based method. The comparison of built models with their reference structures showed some deviations in loop positioning. It suggested the necessity of further structure refinement. Guided by the approach utilized in our previous work [41], we subjected all homology models to Molecular Dynamics simulation with the Desmond module [47]. Using System Builder, models were placed in an orthorhombic box of minimal size and solved with the single-point charge (SPC) water molecules. The imitation systems were neutralized with Cl^- or Na^+ as counterions. Before the actual launch, systems went through the standard eight-step Desmond relaxation protocol. We used the OPLS3e force field. The models were simulated during 100 ns with a 25 ps recording time step using the NPT ensemble class (T=300 K, p =1.01325 bar). The Simulation Interaction Diagram was further used to analyze MD trajectories evaluating protein root-mean-square deviations (RMSD) and root-mean-square fluctuations (RMSF). All trajectories were clustered, and the most populated clusters were used as final prepared models.

2.2. Ligand Preparation and Molecular Docking

Scientific literature sources [48-55] were used to create a database of 232 natural compounds contained in citrus essential oil. Their 3D structures were retrieved from the PubChem database (https://pubchem.ncbi.nlm.nih.gov/). We employed the LigPrep tool [43] to minimize ligand structures using the OPLS3e force field. The Epik was used to generate possible ionization states at target pH = 7.4 ± 0.00. All structures were additionally subjected to toxicity assessment using a ProTox-II web server [56]. Reference structures and created homology models were used as targets to scan the developed library of natural compounds as potential SARS-CoV-2 spike glycoprotein inhibitors. Grids were generated and centered on the interface of RBD's interactions with the host ACE2 receptor (x: -2, y: -30, z: 0, with a length of 36 Å and a size of the inner box of 10 Å). Ligands were docked to selected receptors flexibly with Extra-Precision (XP) mode and OPLS3e force field using a Glide Module [57]. The ligands were further ranked based on their average docking score for all developed homology models and reference structures. An additional assessment of toxicity was carried out using the SwissTargetPrediction [58] and ADMETlab 2.0 [59] web servers. The top 25 most promising ligand-protein complexes were selected for further investigation.

2.3. Molecular Mechanics and Molecular Dynamics

We used complexes of 25 compounds with the best average docking scores to all RBD structures from XP simulation to execute MM-GBSA calculations in the Prime module, leveraging the VSGB solvation model and the OPLS3e force field. Protein residues were flexible up to a 12.0 Å distance for all ligands. Rankings of the protein-ligand complexes were determined by their predicted binding free energy averages. After molecular mechanics, the produced poses underwent molecular dynamics simulations. Complexes were positioned in a minimized orthorhombic box and solvated with SPC water molecules. Chlorine anions were added to neutralize complexes. Desmond's default eight-step relaxation protocol was applied before the main 100 ns simulation with the 25 ps step. The OPLS3e force field was used for all simulations. Lastly, we assessed RMSD, RMSF, and ligand-protein interactions using Simulation Interaction Diagrams.

3. RESULTS AND DISCUSSION

3.1. Homology Models of Omicron RBD Mutants

Based on the 3D structure of the reference Omicron spike glycoprotein RBD, we successfully built ten homology models of mutated clades 21K, 21L, 22A, 22B, 22C, 22D, 22E, 22F, 23C, and newly emerged 23F. Among all selected mutants, some mutations were persistent and characteristic of the Omicron variant (Table **1**). For example, for all clades of Omicron, the following mutations were present: S373P, S375F, K417N, N440K, S477N, T478K, E484A, Q498R, N501Y, and Y505H. The other sets of persistent mutations include T376A, D405N, and R408S, characteristic for all the clades except 21K. Common for Omicron mutation, G339D was altered by G339H in the case of clades 22D, 22F, and all further clades (23C and 23F, in this investigation). The other mutations varied from clade to clade. It must be noted that the reference structures 7T9L and 7XAZ both represent the RBD structure of a virus from the 21K clade; however, these mutants belong to different Pangolin lineage of viruses (BA.1 and BA.1.1, respectively). Thus, the latest one has an R346K mutation, which is not common for other subvariants. All models were refined with molecular dynamics simulation followed by further trajectory clustering. Fig. (**1**) illustrates the results of molecular dynamics simulations and refined 3D structures of developed RBD's homology models.

The models of 21L, 22A, 22B, 23C, and 23F were the most stable, with root mean square deviations (RMSD) not exceeding 2 Å throughout the simulation (Fig. **1a**). The largest deviations in the secondary structure were observed for the 22D model. It stabilized only after a 110 ns run, with deviations at an initial stage of simulations exceeding 7 Å. Mostly, it was associated with fluctuations in the loop between residues L455 and P488, as one can see from root

Table 1. The list of occurred receptor binding domain mutations in selected Omicron clades of SARS-CoV-2.

#	339	346	356	368	371	373	375	376	405	408	417	440	444	445	446	448	452	456	460	477	478	484	486	490	493	494	496	498	501	505
Wild Type	G	R	K	L	S	S	S	T	D	R	K	N	K	V	G	N	L	F	N	S	T	E	F	F	Q	S	G	Q	N	Y
21K	D	K	-	-	L	P	F	-	-	-	N	K	-	-	S	-	-	-	-	N	K	A	-	-	R	-	S	R	Y	H
21L	D	-	-	-	F	P	F	A	N	S	N	K	-	-	-	-	-	-	-	N	K	A	-	-	R	-	-	R	Y	H
22A	D	T	-	-	F	P	F	A	N	S	N	K	-	-	-	-	R	-	-	N	K	A	V	-	-	-	-	R	Y	H
22B	D	-	-	-	F	P	F	A	N	S	N	K	-	-	-	-	R	-	-	N	K	A	V	-	-	-	-	R	Y	H
22C	D	-	-	-	F	P	F	A	N	S	N	K	-	-	-	-	Q	-	-	N	K	A	-	-	R	-	-	R	Y	H
22D	H	T	T	-	F	P	F	A	N	S	N	K	-	-	S	-	-	-	K	N	K	A	S	S	-	P	-	R	Y	H
22E	D	T	-	-	F	P	F	A	N	S	N	K	T	-	-	-	R	-	K	N	K	A	V	-	-	-	-	R	Y	H
22F	H	T	-	I	F	P	F	A	N	S	N	K	-	P	S	-	-	-	K	N	K	A	P	S	-	-	-	R	Y	H
23C	H	T	-	-	F	P	F	A	N	S	N	K	T	-	S	K	R	-	K	N	K	A	S	-	K	-	-	R	Y	H
23F	H	T	-	I	F	P	F	A	N	S	N	K	-	P	S	-	-	L	K	N	K	A	P	S	-	-	-	R	Y	H

Note: * "-" indicates no mutation from the original sequence.

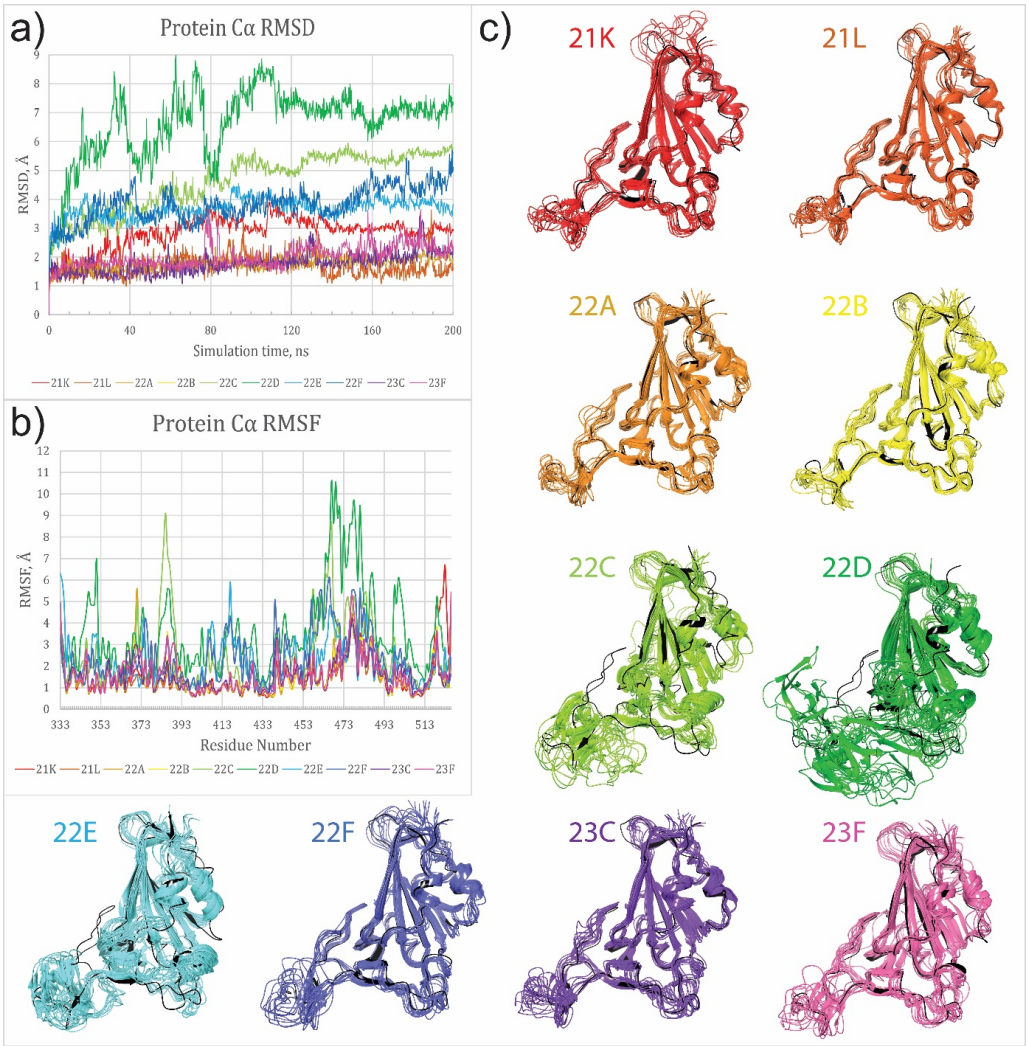

Fig. (1). The results of 3D structures of reference spike glycoprotein RBDs and created homology models: **a**) Protein root mean square deviation plots (RMSD); **b**) Protein root mean square fluctuations (RMSF); **c**) Superposition of ten most populated clusters from MD trajectories of built homology models (in corresponding colors) and their reference structures (in black). Reference structures included the following PDB ID: 7XAZ (for 21K), 7XB0 (for 21L), 7XWA (for 22B), 7XNS (for 22C), and 8IF2 (for 22E), 7T9L (for all other clades as their reference structures are not available yet). *(A higher resolution / colour version of this figure is available in the electronic copy of the article).*

mean square fluctuation (RMSF) plots (Fig. **1b**). Similarly, the model of 22C underwent major conformational changes before it was fully stabilized after 120 ns, with the region near residue N385 being characterized by the most fluctuations. A superposition of the ten most populated clusters from molecular trajectory with reference structures is illustrated in Fig. (**1c**). Models 21K, 21L, and 22B showed the best reproductivity when compared to the corresponding reference structures. Even though the reference structures for 22A, 22F, 23C, and 23F were not available, the comparison of their homology models with other crystallographic Omicron RBDs' structures showed high similarity in secondary structure and geometry. Models 22C, 22D, and 22E showed a significantly different position of the loop between residues L455 and P488 (bottom-left corner of protein structure in Fig. **1c**), similar to model 22F. We did not find any specific trends in 22C, 22D, 22E, and 22F mutations, which could cause this geometry deviation during homology modeling; rather, it could be caused by an additive influence of each mutation that occurred. All developed homology models, as well as all reference structures, were used for further molecular docking, mechanics, and dynamics study.

3.2. Molecular Docking, MM/GBSA and Toxicity Prediction

Molecular docking was performed for all 232 compounds against all target mutants and reference structures. Our goal was to find compounds with equally high docking scores for all mutants. Thus, docking scores of each compound towards each mutant RBD were averaged to make a ranking of ligands. The results for the top 25 compounds based on the averaged docking score are illustrated in Fig. (**2**) as a heatmap. Interestingly, almost all selected ligands docked well to the 21L, 22A, and 22F homology models, while the docking scores for homology model 22E and the reference 7T9L structure were significantly inferior. One can see almost no correlation when comparing docking score trends between homology models and their corresponding reference structures. Molecular docking allows the flexibility of a ligand. However, it does not take into consideration the flexibility of the protein's residues. Homology models, even with high similarity in the backbone geometry, may have varying side-chain positions, which subsequently may influence docking results significantly. That is why we decided to implement molecular mechanics with generalized Born and surface area solvation (MM/GBSA). This approach is commonly used to estimate relative binding affinities. While the absolute calculated values are not always in agreement with experimental data, the ranking of the ligands based on the calculated binding energies is expected to agree reasonably well with the ranking based on experimental binding affinities. The results of the binding energy calculations Fig. (**2**) showed a significant improvement in ligands' activity correlation between homology models and their corresponding reference structures, with 21K, 21L, and 22B models showing the best agreement of results with reference RBDs.

Nonetheless, the data obtained for models 22C and 22E still lack consistency with their crystallographic counterparts. Insufficient performance of these models most probably related to improper geometry, as it was shown in Fig. (**1**) and discussed in the previous subsection. The ligand with PubChem ID: 11230 (terpinen-4-ol or 4-carvomenthenol) was found as the best-scoring compound on average for all clades, followed by p-Cymen-8-ol (PubChem ID: 14529) and 2,7-Cyclodecadien-1-ol, (PubChem ID: 522445). Most of the hit ligands bound strongly to 7T9L, while the worst average binding was noticed for reference 22C structure (noted in Fig. (**2**) as 22C*, PDB ID: 7XNS). Top-scoring terpinen-4-ol mostly showed the comparable binding affinity for both homology models and their corresponding crystallographic structures, except for the 22E clade, where its binding energy with the reference structure (22E*) was significantly higher compared to the 22E homology model.

A more detailed analysis of the MM/GBSA results revealed that terpinen-4-ol has the same binding modes for all RBDs except for homology models 22C, 22D, and 22E (Fig. **3**). The ligand binding was reinforced by a hydrogen bond formed between the hydroxyl group of a ligand and F490 residue (S490 in the case of 22F and 23F). For 22C, 22D, and 22E models, this binding is obstructed due to the specific orientation of the loop. Keeping this in mind and referring to the results of homology modeling, we can say that the above-mentioned models are insufficient for further investigations and must be further refined.

Toxicity prediction using ProTox-II webserver was performed to provide an additional selection criterion (Fig. **4**). While the larger portion of top-scoring compounds (14 out of 25) was predicted to be safe, a few potential ligands were shown as active in toxicity endpoints, such as carcinogenicity, immunotoxicity, cytotoxicity, and Mitochondrial Membrane Potential (MMP). The least promising natural compound was furfural (PubChem ID: 7362), with the lowest value of LD50, the highest toxicity class, and predicted as potentially carcinogenic and mutagenic. Indeed, experimental studies showed that furfural had carcinogenic and genotoxic effects on humans and rats [60-62]. An interesting toxicity profile was predicted for b-Cyclocitral (PubChem ID: 9895). Being inactive in the majority of toxicity endpoints, it showed mitochondrial membrane potential activity and potency of being an aromatase and estrogen receptor (ER-LBD) inhibitor. This indicates its potency as an anticancer drug.

The p-Cymen-8-ol (PubChem ID: 14529), which was scored as a second, had the potential of being carcinogenic. The top-scoring ligand terpinen-4-ol (PubChem ID: 11230) and the third-best-scoring 2,7-Cyclodecadien-1-ol (PubChem ID: 522445) were both predicted to be non-toxic. The terpinen-4-ol is a terpineol that has a role as a plant metabolite and possesses antibacterial, antioxidant, anti-inflammatory, antiparasitic, and antineoplastic activities [63-65]. Additionally, it must be noted that some computational studies highlighted the potency of terpinen-4-ol as an inhibitor of SARS-CoV-2 Main Protease [66] and Wild-type spike glycoprotein RBD [67, 68]. Considering this and its more favorable toxicity profile (Fig. **4**), we selected this natural terpineol for further elucidation as a potential inhibitor of the Omicron RBD.

3.3. Molecular Dynamics Simulation

In order to assess terpinen-4-ol's binding to Omicron RBD, we performed a molecular dynamics simulation. Complexes with 21K (PDB ID: 7T9L) and the Wild type

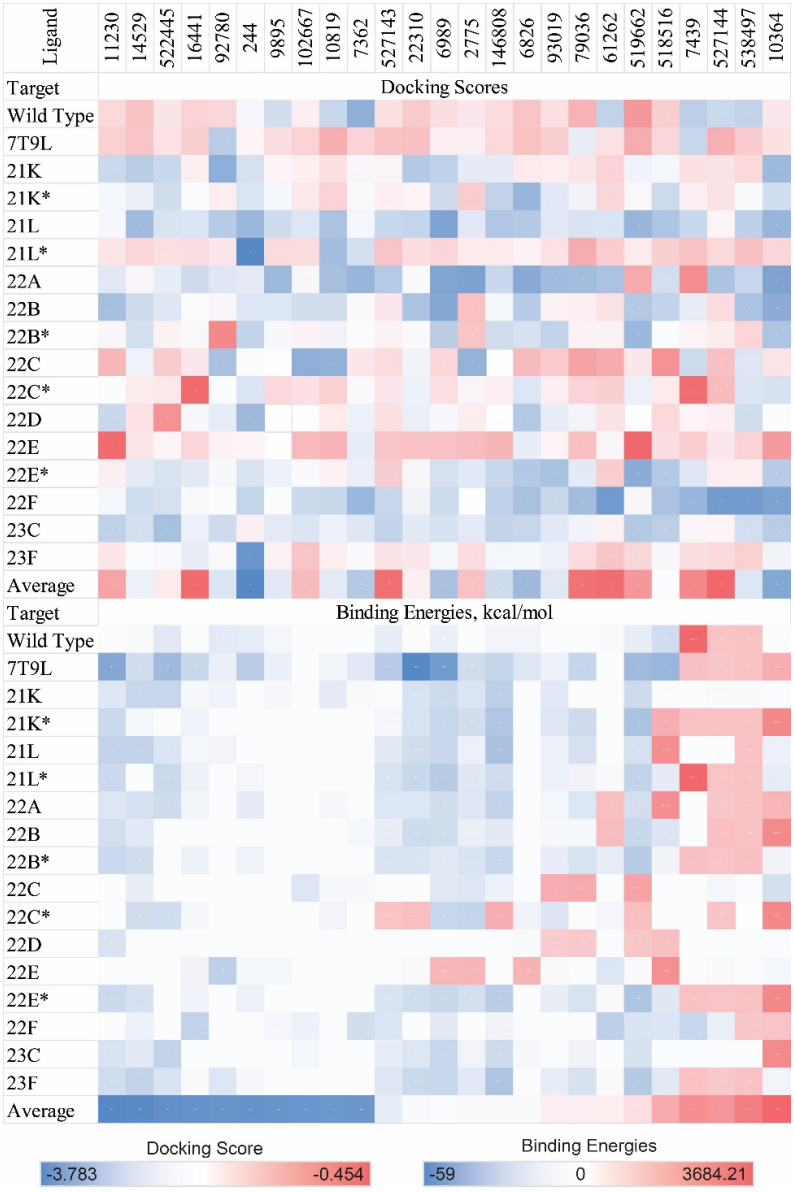

Fig. (2). Heatmaps represent the results of toxicity prediction and molecular docking for the most promising ligands. *indicates the reference structure. *(A higher resolution / colour version of this figure is available in the electronic copy of the article).*

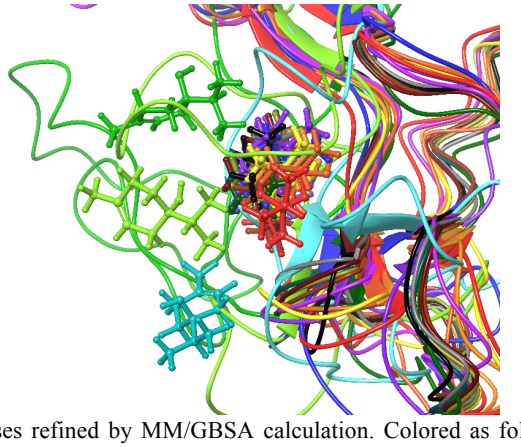

Fig. (3). Superposition of ligand binding poses refined by MM/GBSA calculation. Colored as follows: wild type – black; 21K (PDB ID: 7T9L) – grey; homology models – according to their corresponding colors in Table **1**; other reference structures according to their corresponding colors in Table **1**, but in a darker shade. *(A higher resolution / colour version of this figure is available in the electronic copy of the article).*

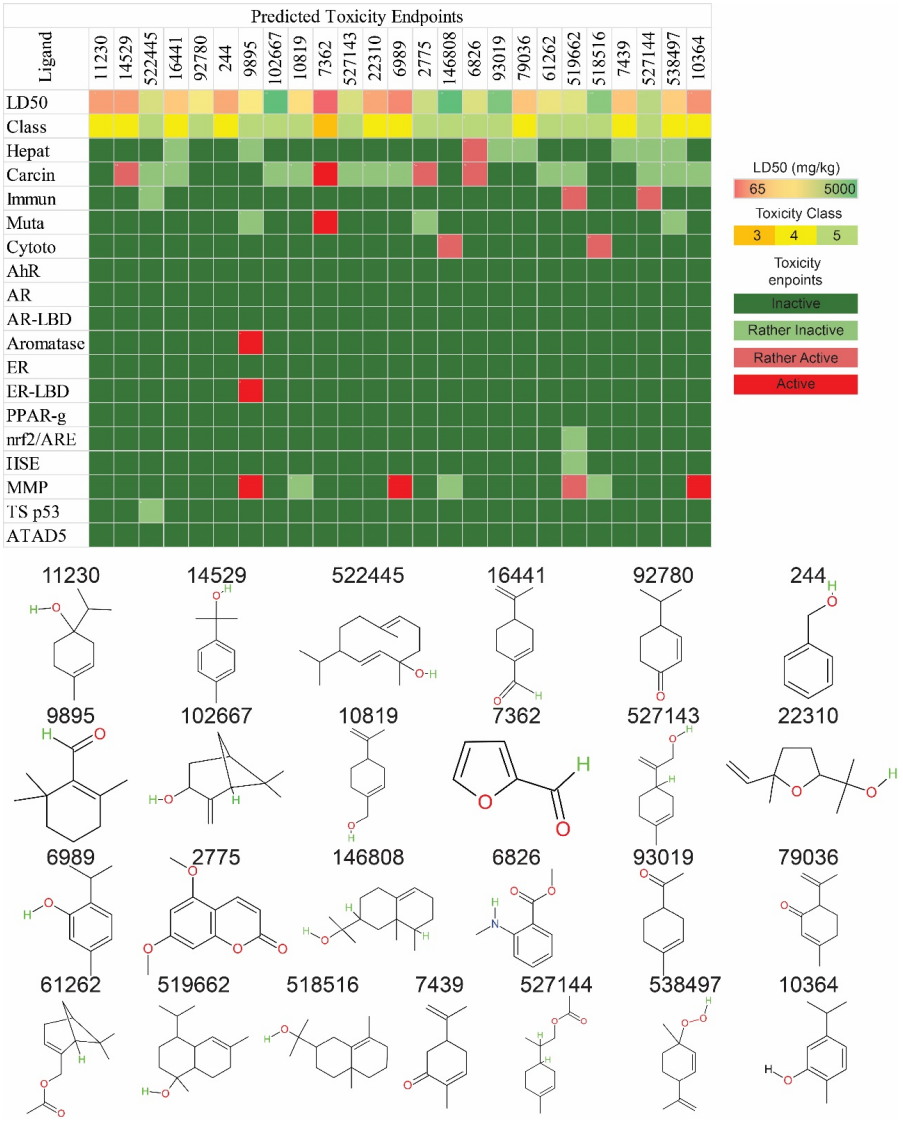

Fig. (4). The top 25 natural compounds best-scoring as inhibitors of an Omicron SARS-CoV-2 RBD and its predicted toxicity profile. *Hepat – hepatotoxicity; Carcin – carcinogenicity, Immun – immunotoxicity; Muta – mutagenicity; Cytoto – cytotoxicity; AhR – Aryl hydrocarbon Receptor; AR – Androgen Receptor; AR-LBD – Androgen Receptor Ligand Binding Domain; ER – Estrogen Receptor; ER-LBD – Estrogen Receptor Ligand Binding Domain; PPAR-g – Peroxisome Proliferator Activated Receptor Gamma; nrf2/ARE – Nuclear factor (erythroid-derived 2)-like 2/antioxidant responsive element; HSE – Heat shock factor response element; MMP – Mitochondrial Membrane Potential; TS p53 – Phosphoprotein (Tumor Suppressor) p53; ATAD5 – ATPase family AAA domain-containing protein 5. *(A higher resolution / colour version of this figure is available in the electronic copy of the article).*

(6M0J) RBDs were used as the most and the least successful targets. Additional simulations were carried out to compare homology model 22E and its corresponding reference structure, considering contradictions in their predicted binding energies. The results of this simulation (Fig. **5**) revealed the sufficient stability of the ligand only within the binding pocket of a 21K (PDB ID: 7T9L) RBD. The deviations in protein RMSD (Fig. **5a**) were relatively low for wild type and 22E reference structure, meanwhile, significant deviations were noted for the reference 21K and 22E homology model. Protein RMSF (Fig. **5b**) for complexes of 21K and 22E reference structures showed insignificant change in residue positions during the simulation, with the only area near residues 478-484 being flexible (up to 4.5 Å). The complex with the wild-type SARS-CoV-2 RBD had an additional flexibility near residues S371, A372, and S373. Overall, large fluctuations were noticed for homology model 22E. Plotting the ligand's RMSD fit on the protein (Fig. **5c**) provided a clearer understanding of the complexes' stability. With both the 22E homology model and crystallographic structure as targets, terpinen-4-ol did not form stable complexes, as shown by the ligand's RMSD ranging up to 80 Å. The ligand complexed with the wild-type RBD showed high deviations at the beginning of the trajectory but stabilized after 30 ns of simulations, which indicated a shift in the ligand's binding site. The most stable was the complex of terpinen-4-ol with 21K RBD, maintaining its deviations near 3 Å from the original frame and its RMSF (Fig. **5d**) not exceeding 1.5 Å. Another measurement used to evaluate the stability of a complex was the radius of gyration (rGyr) (Fig. **5e**),

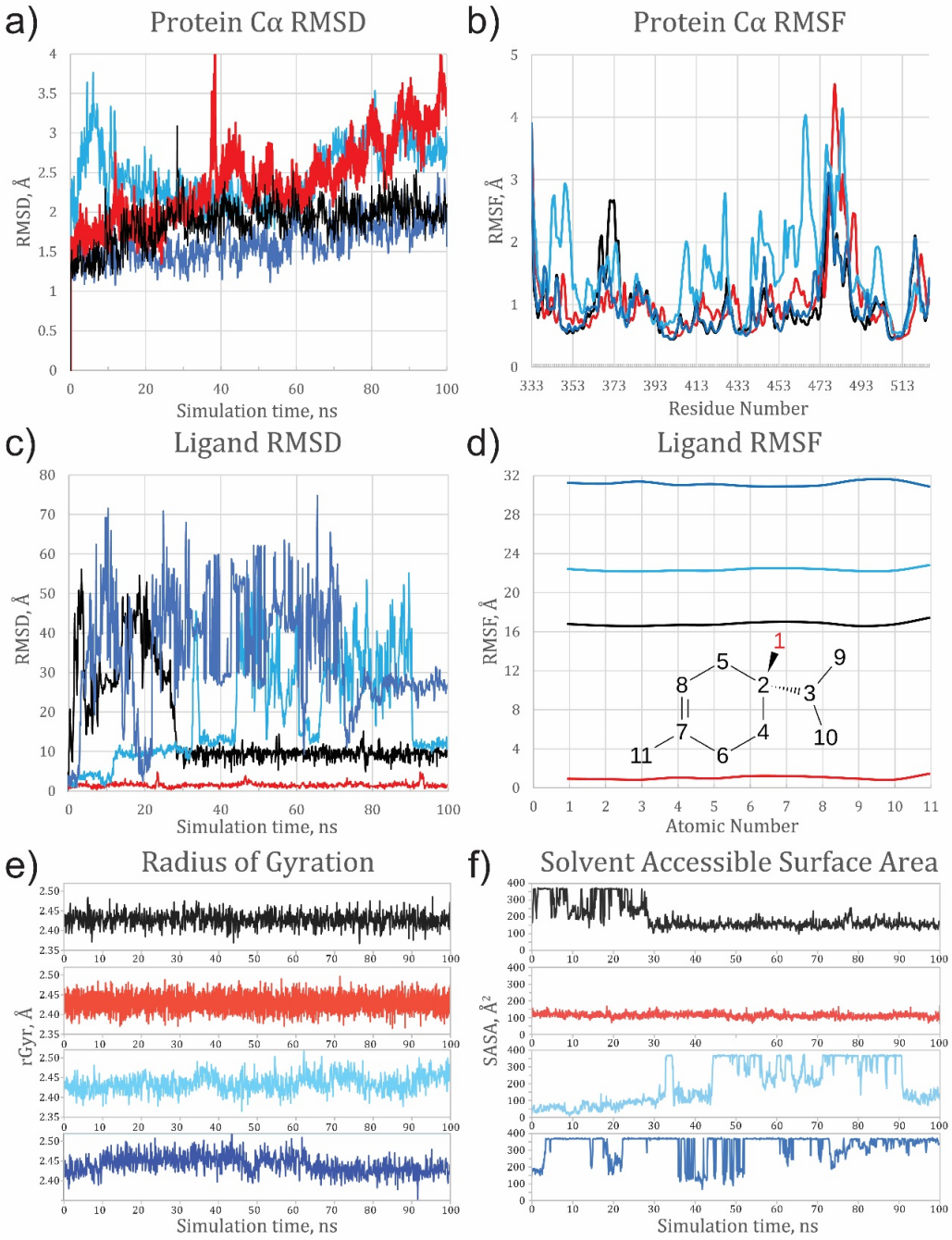

Fig. (5). Results of Molecular Dynamics Simulation for terpinen-4-ol complexes with Wild type (PDB ID: 6M0J, colored black), 21K (PDB ID: 7T9L, colored red), 22E (homology model, colored cyan), and 22E (PDB ID: 8IF2, colored blue): **a**) – protein Ca RMSD; **b**) – Protein Ca RMSF; **c)** – Ligand RMSD fit on protein; **d**) – Ligand RMSF fit on protein; **e**) – Radius of Gyration; **f**) – Solvent Accessible Surface Area. *(A higher resolution / colour version of this figure is available in the electronic copy of the article).*

which assesses the 'extendedness' of a ligand and is equivalent to its principal moment of inertia and solvent assessable surface area (SASA) (Fig. **5f**). According to the radius of gyration, the most compact were the complexes of terpinen-4-ol with the 21K and the wild-type RBDs. Both complexes with 22E showed significant deviations in the extendedness of the ligand, suggesting the instability of these complexes. Solvent assessable surface area for the complex of a wild type RBD decreased significantly after 30 ns simulation, similarly to the Ligand RMSD trend. The smallest exposure to a solvent had a complex of ligands with 21K RBD.

Another good evidence of the complex's stability was obtained by clustering the molecular dynamics simulation. The ten most populated clusters superimposed in Fig. (**6a**) showed the ligand being kept within the same binding site near residues R493, S494, Y495, and S496, which showed a critical role in spike-glycoprotein binding to host ACE2 receptor [41, 69]. As can be seen in the 2D Ligand-Protein Interaction Diagram for this complex Fig. (**6b**), one strong hydrogen bond was formed between the hydroxyl group of terpinen-4-ol (as a donor) and S496 of the Omicron RBD. This bond remained intact within 75% of the simulation

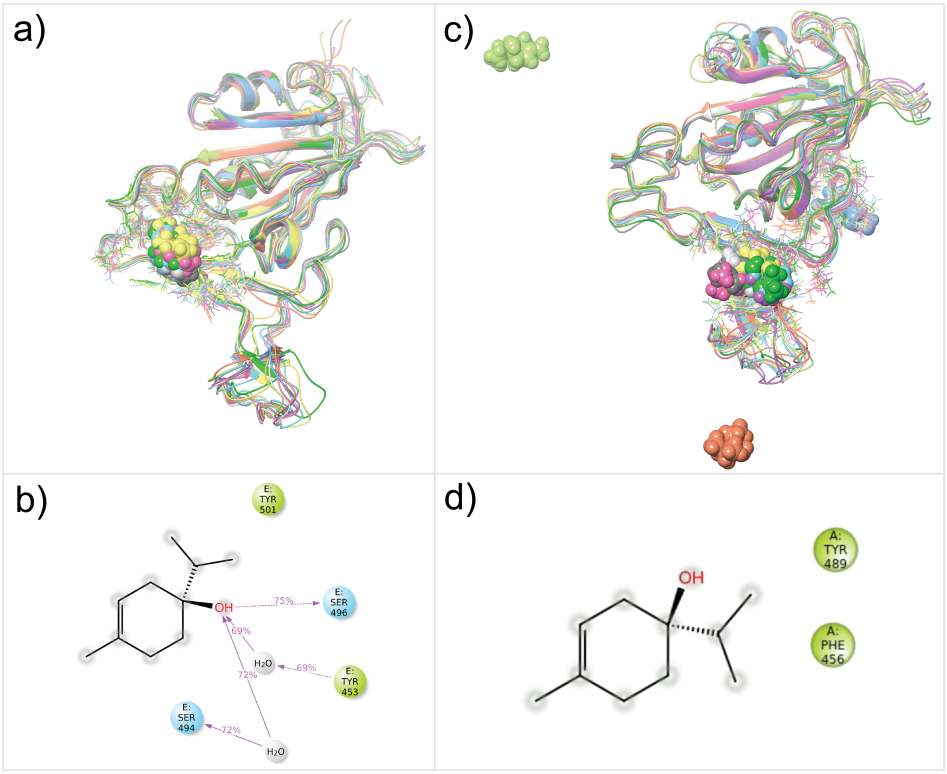

Fig. (6). Results of molecular dynamics simulation for terpinen-4-ol complexes with Omicron (21K clade) RBDs: **a)** - superposition of 10 most populated clusters; **b)** – 2D Ligand-Protein Interaction Diagram; and its complexes with the with wild type RBDs: **c)** - superposition of 10 most populated clusters; **d)** – 2D Ligand-Protein Interaction Diagram (arrows indicate H-bonds). *(A higher resolution / colour version of this figure is available in the electronic copy of the article).*

time. Additional water bridges between the hydroxyl and S494 and Y453 stabilized the complex for 72% and 69% of the simulation time, respectively. The seven out of ten most populated clusters from the molecular dynamics trajectory of the terpinen-4-ol-RBD(wild type) complex (Fig. **6c**) also revealed the ligand being fixed in the same position, located on the interface of RBD-ACE2 interactions. However, it was fixed at this binding pocket solely by hydrophobic interactions (Fig. **6d**) and maintained no hydrogen bonds for longer than 30% of the simulation time. Considering all of the above, the proposed ligand does not look promising as a multivariant inhibitor but rather has the potency of inhibiting SARS-CoV-2 spike glycoprotein from 21K clade with no R346K mutation.

CONCLUSION

The objective of this study was to identify potential inhibitors for the receptor binding domain of the spike glycoprotein of the latest SARS-CoV-2 variant, Omicron. Considering the diverse range of mutant sub-lineages derived from the original Omicron strain, we aimed to evaluate the inhibitory activity of selected compounds against these mutants. Due to the limited availability of 3D structures in the Protein Data Bank, we constructed homology models of the SARS-CoV-2 spike glycoprotein for ten clades of the Omicron variant (21K, 21L, 22A, 22B, 22C, 22D, 22E, 22F, 23C, and 23F. Models were validated by comparing their structures with crystallographic data. All models except for 22C, 22D, and 22E showed high similarity with their corresponding reference structures. This suggested a need for further structure refinement for the three above-mentioned clades. Our previous work [41] demonstrated the inhibitory potential of hesperidin, narirutin, and neohesperidin (all present in citric essential oils) against the RBD of certain SARS-CoV-2 variants (specifically Delta). However, these compounds did not exhibit stable interactions with the RBD of the Omicron variant. To address this, we compiled a database of 232 natural compounds found in citrus essential oils. This library was docked into the developed homology models and studied reference structures of spike glycoprotein. Based on the docking scores, toxicity endpoint predictions, and binding energies predicted using molecular mechanics, terpinen-4-ol emerged as the most potent inhibitor, targeting the RBD of the Omicron strain. A molecular dynamics simulation was conducted to assess the stability of the terpinen-4-ol complex bound to the RBD of the Wild type and certain Omicron strains. The simulation revealed a high degree of stability for the ligand complex with a 21K dereference structure (PDB ID: 7T9L). However, it did not show decent stability in the case of other tested clades. These findings suggested that further extension of the ligand library is needed for the design of potential multivariant inhibitors of the SARS-CoV-2 spike glycoprotein. Even though the library scanned in this work did not yield anticipated results, the methodology proposed here holds promise for further improvements in *in silico* drug discovery targeting viruses with high mutation rates, such as SARS-CoV-2.

LIST OF ABBREVIATIONS

ACE2	=	Angiotensin-converting enzyme 2
ADMET	=	Absorption, Distribution, Metabolism, Excretion, and Toxicity

BBB	=	Blood-brain Barrier
COVID-19	=	Coronavirus Disease of 2019
MD	=	Molecular Dynamics
RBD	=	Receptor-binding Domain
RMSD	=	Root-mean-square Deviations
RMSF	=	Root-mean-square Fluctuations
SARS-CoV-2	=	Severe Acute Respiratory Syndrome Coronavirus 2
VOC	=	Variant of Concern
WHO	=	World Health Organization

ETHICS APPROVAL AND CONSENT TO PARTICIPATE

Not applicable.

HUMAN AND ANIMAL RIGHTS

Not applicable.

CONSENT FOR PUBLICATION

Not applicable.

AVAILABILITY OF DATA AND MATERIALS

The data and supportive information are available within the article.

FUNDING

This work was financially supported by the Mississippi INBRE, funded by an Institutional Development Award (IDeA) from the National Institute of General Medical Sciences of the National Institutes of Health under grant number P20GM103476.

CONFLICT OF INTEREST

The authors declare no conflict of interest, financial or otherwise.

ACKNOWLEDGEMENTS

The content is solely the responsibility of the authors and does not necessarily represent the official views of the National Institutes of General Medical Sciences or the National Institutes of Health.

REFERENCES

[1] Jiang, S.; Shi, Z.; Shu, Y.; Song, J.; Gao, G.F.; Tan, W.; Guo, D. A distinct name is needed for the new coronavirus. *Lancet,* **2020**, *395*(10228), 949. http://dx.doi.org/10.1016/S0140-6736(20)30419-0 PMID: 32087125

[2] Kumari, M.; Lu, R.M.; Li, M.C.; Huang, J.L.; Hsu, F.F.; Ko, S.H.; Ke, F.Y.; Su, S.C.; Liang, K.H.; Yuan, J.P.Y.; Chiang, H.L.; Sun, C.P.; Lee, I.J.; Li, W.S.; Hsieh, H.P.; Tao, M.H.; Wu, H.C. A critical overview of current progress for COVID-19: Development of vaccines, antiviral drugs, and therapeutic antibodies. *J. Biomed. Sci.,* **2022**, *29*(1), 68. http://dx.doi.org/10.1186/s12929-022-00852-9 PMID: 36096815

[3] Thanh Le, T.; Andreadakis, Z.; Kumar, A.; Gómez Román, R.; Tollefsen, S.; Saville, M.; Mayhew, S. The COVID-19 vaccine development landscape. *Nat. Rev. Drug Discov.,* **2020**, *19*(5), 305-306. http://dx.doi.org/10.1038/d41573-020-00073-5 PMID: 32273591

[4] Tanne, J.H. Covid-19: FDA panel votes to authorise Pfizer BioNTech vaccine. *BMJ,* **2020**, *371*, m4799. http://dx.doi.org/10.1136/bmj.m4799 PMID: 33310748

[5] Mahase, E. Covid-19: Moderna applies for US and EU approval as vaccine trial reports 94.1% efficacy. *BMJ,* **2020**, *371*, m4709. http://dx.doi.org/10.1136/bmj.m4709 PMID: 33268462

[6] Costanzo, M.; De Giglio, M.A.R.; Roviello, G.N. Anti-coronavirus vaccines: Past investigations on SARS-CoV-1 and MERS-CoV, the approved vaccines from biontech/pfizer, moderna, oxford/astrazeneca and others under development against SARSCoV-2 infection. *Curr. Med. Chem.,* **2022**, *29*(1), 4-18. http://dx.doi.org/10.2174/1875533XMTE1eNzEw5 PMID: 34355678

[7] Self, W.H.; Tenforde, M.W.; Rhoads, J.P.; Gaglani, M.; Ginde, A.A.; Douin, D.J.; Olson, S.M.; Talbot, H.K.; Casey, J.D.; Mohr, N.M.; Zepeski, A.; McNeal, T.; Ghamande, S.; Gibbs, K.W.; Files, D.C.; Hager, D.N.; Shehu, A.; Prekker, M.E.; Erickson, H.L.; Gong, M.N.; Mohamed, A.; Henning, D.J.; Steingrub, J.S.; Peltan, I.D.; Brown, S.M.; Martin, E.T.; Monto, A.S.; Khan, A.; Hough, C.L.; Busse, L.W.; ten Lohuis, C.C.; Duggal, A.; Wilson, J.G.; Gordon, A.J.; Qadir, N.; Chang, S.Y.; Mallow, C.; Rivas, C.; Babcock, H.M.; Kwon, J.H.; Exline, M.C.; Halasa, N.; Chappell, J.D.; Lauring, A.S.; Grijalva, C.G.; Rice, T.W.; Jones, I.D.; Stubblefield, W.B.; Baughman, A.; Womack, K.N.; Lindsell, C.J.; Hart, K.W.; Zhu, Y.; Mills, L.; Lester, S.N.; Stumpf, M.M.; Naioti, E.A.; Kobayashi, M.; Verani, J.R.; Thornburg, N.J.; Patel, M.M.; Calhoun, N.; Murthy, K.; Herrick, J.; McKillop, A.; Hoffman, E.; Zayed, M.; Smith, M.; Seattle, N.; Ettlinger, J.; Priest, E.; Thomas, J.; Arroliga, A.; Beeram, M.; Kindle, R.; Kozikowski, L-A.; De Souza, L.; Ouellette, S.; Thornton-Thompson, S.; Mehkri, O.; Ashok, K.; Gole, S.; King, A.; Poynter, B.; Stanley, N.; Hendrickson, A.; Maruggi, E.; Scharber, T.; Jorgensen, J.; Bowers, R.; King, J.; Aston, V.; Armbruster, B.; Rothman, R.E.; Nair, R.; Chen, J-T.T.; Karow, S.; Robart, E.; Maldonado, P.N.; Khan, M.; So, P.; Levitt, J.; Perez, C.; Visweswaran, A.; Roque, J.; Rivera, A.; Angeles, L.; Frankel, T.; Angeles, L.; Goff, J.; Huynh, D.; Howell, M.; Friedel, J.; Tozier, M.; Driver, C.; Carricato, M.; Foster, A.; Nassar, P.; Stout, L.; Sibenaller, Z.; Walter, A.; Mares, J.; Olson, L.; Clinansmith, B.; Rivas, C.; Gershengorn, H.; McSpadden, E.J.; Truscon, R.; Kaniclides, A.; Thomas, L.; Bielak, R.; Valvano, W.D.; Fong, R.; Fitzsimmons, W.J.; Blair, C.; Valesano, A.L.; Gilbert, J.; Crider, C.D.; Steinbock, K.A.; Paulson, T.C.; Anderson, L.A.; Kampe, C.; Johnson, J.; McHenry, R.; Blair, M.; Conway, D.; LaRose, M.; Landreth, L.; Hicks, M.; Parks, L.; Bongu, J.; McDonald, D.; Cass, C.; Seiler, S.; Park, D.; Hink, T.; Wallace, M.; Burnham, C-A.; Arter, O.G. Comparative effectiveness of moderna, pfizer-biontech, and janssen (johnson & johnson) vaccines in preventing covid-19 hospitalizations among adults without immunocompromising conditions — United States, March–August 2021. *MMWR Morb. Mortal. Wkly. Rep.,* **2021**, *70*(38), 1337-1343. http://dx.doi.org/10.15585/mmwr.mm7038e1 PMID: 34555004

[8] Williams, T.C.; Burgers, W.A. SARS-CoV-2 evolution and vaccines: Cause for concern? *Lancet Respir. Med.,* **2021**, *9*(4), 333-335. http://dx.doi.org/10.1016/S2213-2600(21)00075-8 PMID: 33524316

[9] To, K.K.W.; Hung, I.F.N.; Ip, J.D.; Chu, A.W.H.; Chan, W.M.; Tam, A.R.; Fong, C.H.Y.; Yuan, S.; Tsoi, H.W.; Ng, A.C.K.; Lee, L.L.Y.; Wan, P.; Tso, E.Y.K.; To, W.K.; Tsang, D.N.C.; Chan, K.H.; Huang, J.D.; Kok, K.H.; Cheng, V.C.C.; Yuen, K.Y. Coronavirus disease 2019 (COVID-19) re-infection by a phylogenetically distinct severe acute respiratory syndrome coronavirus 2 strain confirmed by whole genome sequencing. *Clin. Infect. Dis.,* **2021**, *73*(9), e2946-e2951. http://dx.doi.org/10.1093/cid/ciaa1275 PMID: 32840608

[10] Hossain, M.K.; Hassanzadeganroudsari, M.; Apostolopoulos, V. The emergence of new strains of SARS-CoV-2. What does it mean

for COVID-19 vaccines? *Expert Rev. Vaccines,* **2021**, *20*(6), 635-638.
http://dx.doi.org/10.1080/14760584.2021.1915140 PMID: 33896316

[11] Wu, L.P.; Wang, N.C.; Chang, Y.H.; Tian, X.Y.; Na, D.Y.; Zhang, L.Y.; Zheng, L.; Lan, T.; Wang, L.F.; Liang, G.D. Duration of antibody responses after severe acute respiratory syndrome. *Emerg. Infect. Dis.,* **2007**, *13*(10), 1562-1564.
http://dx.doi.org/10.3201/eid1310.070576 PMID: 18258008

[12] Edridge, A.W.D.; Kaczorowska, J.; Hoste, A.C.R.; Bakker, M.; Klein, M.; Loens, K.; Jebbink, M.F.; Matser, A.; Kinsella, C.M.; Rueda, P.; Ieven, M.; Goossens, H.; Prins, M.; Sastre, P.; Deijs, M.; van der Hoek, L. Seasonal coronavirus protective immunity is short-lasting. *Nat. Med.,* **2020**, *26*(11), 1691-1693.
http://dx.doi.org/10.1038/s41591-020-1083-1 PMID: 32929268

[13] Lippi, G.; Mattiuzzi, C.; Henry, B.M. Neutralizing potency of COVID-19 vaccines against the SARS-CoV-2 Omicron (B.1.1.529) variant. *J. Med. Virol.,* **2022**, *94*(5), 1799-1802.
http://dx.doi.org/10.1002/jmv.27575 PMID: 34988998

[14] Soriano, V.; Fernández-Montero, J.V. New SARS-CoV-2 variants challenge vaccines protection. *AIDS Rev.,* **2021**, *23*(1), 57-58.
http://dx.doi.org/10.24875/AIDSRev.M21000040 PMID: 33750742

[15] Update on Omicron. Available from: https://www.Who.Int/News/Item/28-11-2021-Update-on-Omicron (Accessed June 19 2023.)

[16] Callaway, E. Heavily mutated Omicron variant puts scientists on alert. *Nature,* **2021**, *600*(7887), 21-21.
http://dx.doi.org/10.1038/d41586-021-03552-w PMID: 34824381

[17] Wang, L.; Cheng, G. Sequence analysis of the emerging sars-cov-2 variant omicron in south africa. *J. Med. Virol.,* **2021**.
PMID: 34897752

[18] Karim, S.S.A.; Karim, Q.A. Omicron SARS-CoV-2 variant: A new chapter in the COVID-19 pandemic. *Lancet,* **2021**, *398*(10317), 2126-2128.
http://dx.doi.org/10.1016/S0140-6736(21)02758-6 PMID: 34871545

[19] Du, X.; Tang, H.; Gao, L.; Wu, Z.; Meng, F.; Yan, R.; Qiao, S.; An, J.; Wang, C.; Qin, F.X.F. Omicron adopts a different strategy from Delta and other variants to adapt to host. *Signal Transduct. Target. Ther.,* **2022**, *7*(1), 45.
http://dx.doi.org/10.1038/s41392-022-00903-5 PMID: 35145066

[20] Sigal, A.; Milo, R.; Jassat, W. Estimating disease severity of Omicron and Delta SARS-CoV-2 infections. *Nat. Rev. Immunol.,* **2022**, *22*(5), 267-269.
http://dx.doi.org/10.1038/s41577-022-00720-5 PMID: 35414124

[21] Nyberg, T.; Ferguson, N.M.; Nash, S.G.; Webster, H.H.; Flaxman, S.; Andrews, N.; Hinsley, W.; Bernal, J.L.; Kall, M.; Bhatt, S.; Blomquist, P.; Zaidi, A.; Volz, E.; Aziz, N.A.; Harman, K.; Funk, S.; Abbott, S.; Hope, R.; Charlett, A.; Chand, M.; Ghani, A.C.; Seaman, S.R.; Dabrera, G.; De Angelis, D.; Presanis, A.M.; Thelwall, S.; Nyberg, T.; Ferguson, N.M.; Nash, S.G.; Webster, H.H.; Flaxman, S.; Andrews, N.; Hinsley, W.; Lopez Bernal, J.; Kall, M.; Bhatt, S.; Blomquist, P.; Zaidi, A.; Volz, E.; Abdul Aziz, N.; Harman, K.; Funk, S.; Abbott, S.; Hope, R.; Charlett, A.; Chand, M.; Ghani, A.C.; Seaman, S.R.; Dabrera, G.; De Angelis, D.; Presanis, A.M.; Thelwall, S. Comparative analysis of the risks of hospitalisation and death associated with SARS-CoV-2 omicron (B.1.1.529) and delta (B.1.617.2) variants in England: a cohort study. *Lancet,* **2022**, *399*(10332), 1303-1312.
http://dx.doi.org/10.1016/S0140-6736(22)00462-7 PMID: 35305296

[22] Lewnard, J.A.; Hong, V.X.; Patel, M.M.; Kahn, R.; Lipsitch, M.; Tartof, S.Y. Clinical outcomes associated with SARS-CoV-2 Omicron (B.1.1.529) variant and BA.1/BA.1.1 or BA.2 subvariant infection in Southern California. *Nat. Med.,* **2022**, *28*(9), 1933-1943.
http://dx.doi.org/10.1038/s41591-022-01887-z PMID: 35675841

[23] Cao, Y.; Wang, J.; Jian, F.; Xiao, T.; Song, W.; Yisimayi, A.; Huang, W.; Li, Q.; Wang, P.; An, R. Omicron escapes the majority of existing SARS-CoV-2 neutralizing antibodies. *Nature,* **2021**, 1-9.
PMID: 35016194

[24] Liu, L.; Iketani, S.; Guo, Y.; Chan, J.F.W.; Wang, M.; Liu, L.; Luo, Y.; Chu, H.; Huang, Y.; Nair, M.S. Striking antibody evasion manifested by the omicron variant of SARS-CoV-2. *Nature,* **2021**, 1-8.
PMID: 35016198

[25] Ren, S.Y.; Wang, W.B.; Gao, R.D.; Zhou, A.M. Omicron variant (B.1.1.529) of SARS-CoV-2: Mutation, infectivity, transmission, and vaccine resistance. *World J. Clin. Cases,* **2022**, *10*(1), 1-11.
http://dx.doi.org/10.12998/wjcc.v10.i1.1 PMID: 35071500

[26] Yu, J.; Collier, A.Y.; Rowe, M.; Mardas, F.; Ventura, J.D.; Wan, H.; Miller, J.; Powers, O.; Chung, B.; Siamatu, M.; Hachmann, N.P.; Surve, N.; Nampanya, F.; Chandrashekar, A.; Barouch, D.H. Neutralization of the SARS-CoV-2 Omicron BA.1 and BA.2 Variants. *N. Engl. J. Med.,* **2022**, *386*(16), 1579-1580.
http://dx.doi.org/10.1056/NEJMc2201849 PMID: 35294809

[27] Smith, L.; Shin, J.I.; Koyanagi, A. Vaccine strategy against COVID-19 with a focus on the omicron and stealth omicron variants: Life cycle committee recommendations. *Life Cycle,* **2022**, *2*, e5.
http://dx.doi.org/10.54724/lc.2022.e5

[28] Hadfield, J.; Megill, C.; Bell, S.M.; Huddleston, J.; Potter, B.; Callender, C.; Sagulenko, P.; Bedford, T.; Neher, R.A. Nextstrain: Real-time tracking of pathogen evolution. *Bioinformatics,* **2018**, *34*(23), 4121-4123.
http://dx.doi.org/10.1093/bioinformatics/bty407 PMID: 29790939

[29] Han, P.; Li, L.; Liu, S.; Wang, Q.; Zhang, D.; Xu, Z.; Han, P.; Li, X.; Peng, Q.; Su, C.; Huang, B.; Li, D.; Zhang, R.; Tian, M.; Fu, L.; Gao, Y.; Zhao, X.; Liu, K.; Qi, J.; Gao, G.F.; Wang, P. Receptor binding and complex structures of human ACE2 to spike RBD from omicron and delta SARS-CoV-2. *Cell,* **2022**, *185*(4), 630-640.e10.
http://dx.doi.org/10.1016/j.cell.2022.01.001 PMID: 35093192

[30] Li, L.; Liao, H.; Meng, Y.; Li, W.; Han, P.; Liu, K.; Wang, Q.; Li, D.; Zhang, Y.; Wang, L.; Fan, Z.; Zhang, Y.; Wang, Q.; Zhao, X.; Sun, Y.; Huang, N.; Qi, J.; Gao, G.F. Structural basis of human ACE2 higher binding affinity to currently circulating Omicron SARS-CoV-2 sub-variants BA.2 and BA.1.1. *Cell,* **2022**, *185*(16), 2952-2960.e10.
http://dx.doi.org/10.1016/j.cell.2022.06.023 PMID: 35809570

[31] Jawad, B.; Adhikari, P.; Podgornik, R.; Ching, W.Y. Binding interactions between receptor-binding domain of spike protein and human angiotensin converting enzyme-2 in omicron variant. *J. Phys. Chem. Lett.,* **2022**, *13*(17), 3915-3921.
http://dx.doi.org/10.1021/acs.jpclett.2c00423 PMID: 35481766

[32] Hanai, T. Quantitative *in silico* analysis of SARS-CoV-2 S-RBD omicron mutant transmissibility. *Talanta,* **2022**, *240*, 123206.
http://dx.doi.org/10.1016/j.talanta.2022.123206 PMID: 35026638

[33] Ai, J.; Wang, X.; He, X.; Zhao, X.; Zhang, Y.; Jiang, Y.; Li, M.; Cui, Y.; Chen, Y.; Qiao, R.; Li, L.; Yang, L.; Li, Y.; Hu, Z.; Zhang, W.; Wang, P. Antibody evasion of SARS-CoV-2 Omicron BA.1, BA.1.1, BA.2, and BA.3 sub-lineages. *Cell Host Microbe,* **2022**, *30*(8), 1077-1083.e4.
http://dx.doi.org/10.1016/j.chom.2022.05.001 PMID: 35594867

[34] Cameroni, E.; Bowen, J.E.; Rosen, L.E.; Saliba, C.; Zepeda, S.K.; Culap, K.; Pinto, D.; VanBlargan, L.A.; De Marco, A.; di Iulio, J.; Zatta, F.; Kaiser, H.; Noack, J.; Farhat, N.; Czudnochowski, N.; Havenar-Daughton, C.; Sprouse, K.R.; Dillen, J.R.; Powell, A.E.; Chen, A.; Maher, C.; Yin, L.; Sun, D.; Soriaga, L.; Bassi, J.; Silacci-Fregni, C.; Gustafsson, C.; Franko, N.M.; Logue, J.; Iqbal, N.T.; Mazzitelli, I.; Geffner, J.; Grifantini, R.; Chu, H.; Gori, A.; Riva, A.; Giannini, O.; Ceschi, A.; Ferrari, P.; Cippà, P.E.; Franzetti-Pellanda, A.; Garzoni, C.; Halfmann, P.J.; Kawaoka, Y.; Hebner, C.; Purcell, L.A.; Piccoli, L.; Pizzuto, M.S.; Walls, A.C.; Diamond, M.S.; Telenti, A.; Virgin, H.W.; Lanzavecchia, A.; Snell, G.; Veesler, D.; Corti, D. Broadly neutralizing antibodies overcome SARS-CoV-2 Omicron antigenic shift. *Nature,* **2022**, *602*(7898), 664-670.
http://dx.doi.org/10.1038/s41586-021-04386-2 PMID: 35016195

[35] Xiong, D.; Zhao, X.; Luo, S.; Cong, Y.; Zhang, J.Z.H.; Duan, L. Immune escape mechanisms of SARS-CoV-2 delta and omicron variants against two monoclonal antibodies that received emergency use authorization. *J. Phys. Chem. Lett.,* **2022**, *13*(26), 6064-6073.

http://dx.doi.org/10.1021/acs.jpclett.2c00912 PMID: 35758899

[36] da Costa, C.H.S.; de Freitas, C.A.B.; Alves, C.N.; Lameira, J. Assessment of mutations on RBD in the spike protein of SARS-CoV-2 alpha, delta and omicron variants. *Sci. Rep.,* **2022**, *12*(1), 8540. http://dx.doi.org/10.1038/s41598-022-12479-9 PMID: 35595778

[37] Shi, D.; Bu, C.; He, P.; Song, Y.; Dordick, J.S.; Linhardt, R.J.; Chi, L.; Zhang, F. Structural characteristics of heparin binding to SARS-CoV-2 Spike Protein RBD of omicron sub-lineages BA.2.12.1, BA.4 and BA.5. *Viruses,* **2022**, *14*(12), 2696. http://dx.doi.org/10.3390/v14122696 PMID: 36560700

[38] Singh, S.; Banavath, H.N.; Godara, P.; Naik, B.; Srivastava, V.; Prusty, D. Identification of antiviral peptide inhibitors for receptor binding domain of SARS-CoV-2 omicron and its Sub-Variants: An *in-silico* approach. **2022**, *12*(198) http://dx.doi.org/10.1007/s13205-022-03258-4

[39] Moriyama, S.; Anraku, Y.; Taminishi, S.; Adachi, Y.; Kuroda, D.; Kita, S.; Higuchi, Y.; Kirita, Y.; Kotaki, R.; Tonouchi, K.; Yumoto, K.; Suzuki, T.; Someya, T.; Fukuhara, H.; Kuroda, Y.; Yamamoto, T.; Onodera, T.; Fukushi, S.; Maeda, K.; Nakamura-Uchiyama, F.; Hashiguchi, T.; Hoshino, A.; Maenaka, K.; Takahashi, Y. Structural delineation and computational design of SARS-CoV-2-neutralizing antibodies against Omicron subvariants. *Nat. Commun.,* **2023**, *14*(1), 4198. http://dx.doi.org/10.1038/s41467-023-39890-8 PMID: 37452031

[40] Muhammed, M.T.; Aki-Yalcin, E. Homology modeling in drug discovery: Overview, current applications, and future perspectives. *Chem. Biol. Drug Des.,* **2019**, *93*(1), 12-20. http://dx.doi.org/10.1111/cbdd.13388 PMID: 30187647

[41] Ovchynnykova, O.; Kapusta, K.; Sizochenko, N.; Sukhyy, K.M.; Kolodziejczyk, W.; Hill, G.A.; Saloni, J. Homology modeling and molecular dynamics-driven search for natural inhibitors that universally target receptor-binding domain of spike glycoprotein in SARS-CoV-2 variants. *Molecules,* **2022**, *27*(21), 7336. http://dx.doi.org/10.3390/molecules27217336 PMID: 36364158

[42] Schrödinger Release 2020-3: Schrödinger, LLC, New York, NY, **2020**.

[43] Madhavi Sastry, G.; Adzhigirey, M.; Day, T.; Annabhimoju, R.; Sherman, W. Protein and ligand preparation: Parameters, protocols, and influence on virtual screening enrichments. *J. Comput. Aided Mol. Des.,* **2013**, *27*(3), 221-234. http://dx.doi.org/10.1007/s10822-013-9644-8 PMID: 23579614

[44] Shelley, J.C.; Cholleti, A.; Frye, L.L.; Greenwood, J.R.; Timlin, M.R.; Uchimaya, M. Epik: a software program for pK a prediction and protonation state generation for drug-like molecules. *J. Comput. Aided Mol. Des.,* **2007**, *21*(12), 681-691. http://dx.doi.org/10.1007/s10822-007-9133-z PMID: 17899391

[45] Roos, K.; Wu, C.; Damm, W.; Reboul, M.; Stevenson, J.M.; Lu, C.; Dahlgren, M.K.; Mondal, S.; Chen, W.; Wang, L.; Abel, R.; Friesner, R.A.; Harder, E.D. OPLS3e: Extending force field coverage for drug-like small molecules. *J. Chem. Theory Comput.,* **2019**, *15*(3), 1863-1874. http://dx.doi.org/10.1021/acs.jctc.8b01026 PMID: 30768902

[46] Thompson, J.D.; Gibson, T.J.; Higgins, D.G. Multiple sequence alignment using clustalw and clustalx. *Curr. Protoc. Bioinformatics,* **2003**, *00*(1) http://dx.doi.org/10.1002/0471250953.bi0203s00 PMID: 18792934

[47] Bowers, K.J.; Chow, D.E.; Xu, H.; Dror, R.O.; Eastwood, M.P.; Gregersen, B.A.; Klepeis, J.L.; Kolossvary, I.; Moraes, M.A.; Sacerdoti, F.D. Scalable algorithms for molecular dynamics simulations on commodity clusters. *SC'06: Proceedings of the 2006 ACM/IEEE Conference on Supercomputing,* **2006**, , 43. http://dx.doi.org/10.1109/SC.2006.54

[48] Shaw, P.E. Review of quantitative analyses of citrus essential oils. *J. Agric. Food Chem.,* **1979**, *27*(2), 246-257. http://dx.doi.org/10.1021/jf60222a032

[49] Hosni, K.; Zahed, N.; Chrif, R.; Abid, I.; Medfei, W.; Kallel, M.; Brahim, N.B.; Sebei, H. Composition of peel essential oils from four selected Tunisian Citrus species: Evidence for the genotypic influence. *Food Chem.,* **2010**, *123*(4), 1098-1104. http://dx.doi.org/10.1016/j.foodchem.2010.05.068

[50] Ferhat, M.A.; Meklati, B.Y.; Chemat, F. Comparison of different isolation methods of essential oil from *Citrus* fruits: Cold pressing, hydrodistillation and microwave 'dry' distillation. *Flavour Fragrance J.,* **2007**, *22*(6), 494-504. http://dx.doi.org/10.1002/ffj.1829

[51] Espina, L.; Somolinos, M.; Lorán, S.; Conchello, P.; García, D.; Pagán, R. Chemical composition of commercial citrus fruit essential oils and evaluation of their antimicrobial activity acting alone or in combined processes. *Food Control,* **2011**, *22*(6), 896-902. http://dx.doi.org/10.1016/j.foodcont.2010.11.021

[52] Dosoky, N.; Setzer, W. Biological activities and safety of *citrus* spp. essential oils. *Int. J. Mol. Sci.,* **2018**, *19*(7), 1966. http://dx.doi.org/10.3390/ijms19071966 PMID: 29976894

[53] Choi, H.S.; Song, H.S.; Ukeda, H.; Sawamura, M. Radical-scavenging activities of citrus essential oils and their components: Detection using 1,1-diphenyl-2-picrylhydrazyl. *J. Agric. Food Chem.,* **2000**, *48*(9), 4156-4161. http://dx.doi.org/10.1021/jf000227d PMID: 10995330

[54] Bora, H.; Kamle, M.; Mahato, D.K.; Tiwari, P.; Kumar, P. *Citrus* essential oils (CEOs) and their applications in food: An overview. *Plants,* **2020**, *9*(3), 357. http://dx.doi.org/10.3390/plants9030357 PMID: 32168877

[55] Ambrosio, C.M.S.; Ikeda, N.Y.; Miano, A.C.; Saldaña, E.; Moreno, A.M.; Stashenko, E.; Contreras-Castillo, C.J.; Da Gloria, E.M. Unraveling the selective antibacterial activity and chemical composition of citrus essential oils. *Sci. Rep.,* **2019**, *9*(1), 17719. http://dx.doi.org/10.1038/s41598-019-54084-3 PMID: 31776388

[56] Banerjee, P.; Eckert, A.O.; Schrey, A.K.; Preissner, R. ProTox-II: A webserver for the prediction of toxicity of chemicals. *Nucleic Acids Res.,* **2018**, *46*(W1), W257-W263. http://dx.doi.org/10.1093/nar/gky318 PMID: 29718510

[57] Friesner, R.A.; Murphy, R.B.; Repasky, M.P.; Frye, L.L.; Greenwood, J.R.; Halgren, T.A.; Sanschagrin, P.C.; Mainz, D.T. Extra precision glide: Docking and scoring incorporating a model of hydrophobic enclosure for protein-ligand complexes. *J. Med. Chem.,* **2006**, *49*(21), 6177-6196. http://dx.doi.org/10.1021/jm051256o PMID: 17034125

[58] Daina, A.; Michielin, O.; Zoete, V. SwissTargetPrediction: updated data and new features for efficient prediction of protein targets of small molecules. *Nucleic Acids Res.,* **2019**, *47*(W1), W357-W364. http://dx.doi.org/10.1093/nar/gkz382 PMID: 31106366

[59] Xiong, G.; Wu, Z.; Yi, J.; Fu, L.; Yang, Z.; Hsieh, C.; Yin, M.; Zeng, X.; Wu, C.; Lu, A.; Chen, X.; Hou, T.; Cao, D. ADMETlab 2.0: An integrated online platform for accurate and comprehensive predictions of ADMET properties. *Nucleic Acids Res.,* **2021**, *49*(W1), W5-W14. http://dx.doi.org/10.1093/nar/gkab255 PMID: 33893803

[60] Park, H.S.; Um, Y.; Sim, S.J.; Lee, S.Y.; Woo, H.M. Transcriptomic analysis of Corynebacterium glutamicum in the response to the toxicity of furfural present in lignocellulosic hydrolysates. *Process Biochem.,* **2015**, *50*(3), 347-356. http://dx.doi.org/10.1016/j.procbio.2014.11.014

[61] Gupta, G.D.; Misra, A.; Agarwal, D.K. Inhalation toxicity of furfural vapours: An assessment of biochemical response in rat lungs. *J. Appl. Toxicol.,* **1991**, *11*(5), 343-347. http://dx.doi.org/10.1002/jat.2550110508 PMID: 1783739

[62] Castellino, N.; Elmino, O.; Rozera, G. Experimental research on toxicity of furfural. *Arch. Environ. Health,* **1963**, *7*(5), 574-582. http://dx.doi.org/10.1080/00039896.1963.10663586 PMID: 14058824

[63] Shapira, S.; Pleban, S.; Kazanov, D.; Tirosh, P.; Arber, N. Terpinen-4-ol: A novel and promising therapeutic agent for human gastrointestinal cancers. *PLoS One,* **2016**, *11*(6), e0156540. http://dx.doi.org/10.1371/journal.pone.0156540 PMID: 27275783

[64] Morcia, C. *In Vitro* antifungal activity of terpinen-4-Ol, eugenol, carvone, 1,8-Cineole (Eucalyptol) and thymol against mycotoxigenic plant pathogens. *Food Additives & Contaminants,* **2011**, 1-8. http://dx.doi.org/10.1080/19440049.2011.643458

[65] Zhang, Y.; Feng, R.; Li, L.; Zhou, X.; Li, Z.; Jia, R.; Song, X.; Zou, Y.; Yin, L.; He, C.; Liang, X.; Zhou, W.; Wei, Q.; Du, Y.; Yan, K.; Wu, Z.; Yin, Z. The antibacterial mechanism of terpinen-4-ol

against streptococcus agalactiae. *Curr. Microbiol.,* **2018**, *75*(9), 1214-1220.
http://dx.doi.org/10.1007/s00284-018-1512-2 PMID: 29804206

[66] Muhammad, I.A.; Muangchoo, K.; Muhammad, A.; Ajingi, Y.S.; Muhammad, I.Y.; Umar, I.D.; Muhammad, A.B. A computational study to identify potential inhibitors of SARS-CoV-2 main protease (Mpro) from eucalyptus active compounds. *Computation,* **2020**, *8*(3), 79.
http://dx.doi.org/10.3390/computation8030079

[67] Rout, J.; Swain, B.C.; Tripathy, U. *In silico* investigation of spice molecules as potent inhibitor of SARS-CoV-2. *J. Biomol. Struct. Dyn.,* **2022**, *40*(2), 860-874.
http://dx.doi.org/10.1080/07391102.2020.1819879 PMID: 32938313

[68] Romeo, A.; Iacovelli, F.; Scagnolari, C.; Scordio, M.; Frasca, F.; Condò, R.; Ammendola, S.; Gaziano, R.; Anselmi, M.; Divizia, M.; Falconi, M. Potential use of tea tree oil as a disinfectant agent against coronaviruses: A combined experimental and simulation study. *Molecules,* **2022**, *27*(12), 3786.
http://dx.doi.org/10.3390/molecules27123786 PMID: 35744913

[69] Ali, A.; Vijayan, R. Dynamics of the ACE2–SARS-CoV-2/SARS-CoV spike protein interface reveal unique mechanisms. *Sci. Rep.,* **2020**, *10*(1), 14214.
http://dx.doi.org/10.1038/s41598-020-71188-3 PMID: 32848162